

Anomalous x-ray scattering study of $\text{Ge}_x\text{Se}_{1-x}$ glassy alloys across the stiffness transition composition

Shinya Hosokawa*

Center for Materials Research Using Third-Generation Synchrotron Radiation Facilities, Hiroshima Institute of Technology,
Hiroshima 731-5193, Japan

Physikalische Chemie, Fachbereich Chemie, Philipps Universität Marburg, D-35032 Marburg, Germany

Isamu Oh†

Handai Frontier Research Center, Graduate School of Engineering, Osaka University, Suita 565-0871, Japan

Masaki Sakurai

Institute for Materials Research, Tohoku University, Sendai 980-8577, Japan

Wolf-Christian Pilgrim

Physikalische Chemie, Fachbereich Chemie, Philipps Universität Marburg, D-35032 Marburg, Germany

Nathalie Boudet and Jean-François Béar

Institut Néel, CNRS/UJF, F-38042 Grenoble Cedex 9, France

Shinji Kohara

Research and Utilization Division, Japan Synchrotron Radiation Research Institute (JASRI/SPring-8), Hyogo 679-5198, Japan

(Received 25 October 2010; revised manuscript received 21 March 2011; published 27 July 2011)

Anomalous x-ray scattering experiments on glassy $\text{Ge}_x\text{Se}_{1-x}$ were carried out at energies close to the Ge and Se K absorption edges at concentrations between $x = 0.15$ and 0.333 in order to explore the correlation between the atomic structures in short and intermediate ranges and the stiffness transition which appears at approximately $x = 0.20$ in this glassy system. The partial structure factors $S_{ij}(Q)$ and the corresponding partial pair-distribution functions $g_{ij}(r)$ were obtained using reverse Monte Carlo modeling. Although the $S_{ij}(Q)$ and $g_{ij}(r)$ spectra seem to gradually change with x , some indications are found related to the stiffness transition, in particular in the intermediate-range structure. First, the preshoulder position in $S_{\text{SeSe}}(Q)$ largely shifts toward lower Q values in the *intermediate phase* concentration region of the stiffness transition, while the prepeak positions in $S_{\text{GeGe}}(Q)$ and $S_{\text{GeSe}}(Q)$ remain almost unchanged. Second, the Ge-Se-Se bond angles are distributed at $\sim 90^\circ$ when the transition region is approached with decreasing x . No appreciable portions of the Ge-Se-Se-Ge sequences, i.e., $\text{Ge}(\text{Se}_{1/2})_4$ tetrahedra connected by the Se_2 dimer, are found in the $\text{Ge}_{0.20}\text{Se}_{0.80}$ glass. Instead, there is experimental evidence for a phase-separation tendency between directly connected $\text{Ge}(\text{Se}_{1/2})_4$ tetrahedra and Se_n ($n \geq 3$) chains in the *intermediate phase* concentration region of the stiffness transition. This may be due to avoid large stress in the Se_2 dimer bonds of the Ge-Se-Se bond angle.

DOI: [10.1103/PhysRevB.84.014201](https://doi.org/10.1103/PhysRevB.84.014201)

PACS number(s): 61.05.cf, 61.43.Fs

I. INTRODUCTION

Mean-field constraint theory^{1,2} for network glasses is a powerful tool for explaining numerous experimentally observed anomalies around the critical composition of the rigidity percolation threshold occurring at an average coordination number $\langle r_c \rangle = 2.40$. There, the number of constraints per atom is equal to the degree of freedom. In the case of glassy $\text{Ge}_x\text{Se}_{1-x}$ systems, this corresponds to $x = 0.20$. The character of the network glass undergoes a steep first-order-like transition from easily deformable (floppy) at $\langle r_c \rangle < 2.40$ to rigid at $\langle r_c \rangle > 2.40$. Kamitakahara *et al.*³ reported a vibrational density of states at ~ 5 meV to prove the existence of the floppy mode (zero-frequency mode in the floppy glasses) by inelastic neutron scattering. Ultraviolet photoemission and inverse-photoemission measurements⁴ indicated that the valence- and conduction-band electronic density of states shows abrupt concentration changes from glassy Se like to glassy GeSe_2 like around the transition composition.

Boolchand and co-workers^{5,6} demonstrated that results from Raman scattering, modulated scanning calorimetry, and Mössbauer spectroscopy measured in fine concentration steps provide evidence for a multiplicity of stiffness transitions with an onset point near $\langle r_c \rangle = 2.40$ ($x = 0.20$) and a completion point near $\langle r_c \rangle = 2.52$ ($x = 0.26$). Of particular interest are the Raman-scattering results that showed a shift of the corner-sharing mode frequency for the $\text{Ge}(\text{Se}_{1/2})_4$ tetrahedral units with varying x . The data indicate a second-order transition (kink) from a floppy to an unstressed-rigid phase at $x = 0.20$, and a first-order transition (jump) from the unstressed-rigid to a stressed-rigid phase at $x = 0.26$. This unstressed-rigid concentration range ($0.20 \leq x \leq 0.26$) is called an *intermediate phase*. The interpretations of the Raman-scattering result should also correlate with the atomic structure of glassy $\text{Ge}_x\text{Se}_{1-x}$ around these stiffness threshold compositions.

X-ray-absorption fine-structure (XAFS) spectroscopy provides excellent information on local structure in the first

coordination shell, or the so-called short-range order (SRO), around each constituent element. Therefore, precise studies of the concentration dependence of the atomic structure of glassy $\text{Ge}_x\text{Se}_{1-x}$ were performed in the concentration range $0 \leq x \leq 0.333$.⁷⁻⁹ The experiments confirmed the predicted coordination numbers of the $8 - N$ rule with a bond length similar to that in the crystal, and only Ref. 9 suggested minor deviations from that rule. Structural information beyond the SRO is, however, very limited due to the short lifetime of photoexcited electrons during the XAFS process. It should also be noted that due to similar backscattering amplitudes and phase-shift functions of Ge and Se, it is hard to discriminate Ge neighbors from Se atoms and vice versa.

An x-ray scattering study was performed in the range $0 \leq x \leq 0.25$,¹⁰ in concentration steps of ~ 0.05 . It was found that the structure factor $S(Q)$ comprises a prepeak at approximately $Q = 11 \text{ nm}^{-1}$. The prepeak, being clear evidence for the existence of an intermediate-range order (IRO), shows a systematic decrease in intensity and shifts toward higher Q values with decreasing x . An earlier x-ray scattering experiment,¹¹ as well as a later neutron-diffraction measurement,¹² indicated the same concentration variation of the prepeak. Wang *et al.*¹³ carried out x-ray scattering measurements in an even wider concentration range ($x = 0.07\text{--}0.333$) in finer steps of $0.005\text{--}0.05$ to carefully explore the relation between the IRO and the stiffness transition. It was found that with decreasing x , the prepeak position starts to deviate from a linear relation near the onset of the transition at $x = 0.20$. There, the area under the prepeak which is associated with the Ge-Ge correlation has a plateau with decreasing x followed by a rapid decrease at $x < 0.18$.

Another x-ray scattering study was performed by Sharma *et al.*,¹⁴ who also observed structural anomalies on intermediate length scales around the stiffness transition region. The results are, however, inconsistent with those by Wang *et al.*¹³ Although prepeak positions and widths show a plateau in the concentration dependence, it was not observed in the x dependence of the prepeak area. The discrepancies may, however, originate from the fact that Sharma *et al.* did not take the Se-Se contribution in the prepeak into account as Wang *et al.* did.

Recently, Shatnawi *et al.*¹⁵ carried out high-energy x-ray scattering and XAFS measurements on 18 closely spaced compositions of $\text{Ge}_x\text{Se}_{1-x}$ glasses with $0.15 \leq x \leq 0.40$ to search for a structural response to the intermediate phase ($0.20 \leq x \leq 0.26$) in these glasses. However, the parameters obtained from these experiments smoothly evolve with x , and there are no clear discontinuities or breaks in the slope associated with the appearance of the intermediate phase. Therefore, it was concluded that these measurements do not confirm a structural origin for the intermediate phase. Thus, a further experiment is necessary, from which partial information on the IRO can be obtained, and which allows to discuss the structural origin of the stiffness transition in detail.

Anomalous x-ray scattering (AXS) is a noble method¹⁶⁻¹⁸ that can provide information on both the SRO and IRO around each constituent element. Such an experiment was carried out by Armand *et al.*¹⁹ at $x = 0.25$ and 0.167 . From the differential structure factors $\Delta_i S(Q)$, which are obtained from the AXS measurement, they concluded that the structure at

$x = 0.25$ is based on crystalline GeSe_2 consisting of edge- and corner-sharing $\text{Ge}(\text{Se}_{1/2})_4$ tetrahedra. At $x = 0.167$, on the other hand, the structure is built up of isolated $\text{Ge}(\text{Se}_{1/2})_4$ tetrahedra interconnected by short Se chains. Moreover, they suggested that the prepeak seems to be due to the Ge-Ge correlations, which Petri *et al.*²⁰ also pointed out on glassy GeSe_2 by measuring neutron-scattering using isotope substitution (NDIS).

Hosokawa *et al.*²¹ carried out an AXS experiment at $x = 0.23$ and 0.195 , which are respectively close to the mid- and onset point concentrations of Boolchand's criterion.⁶ The prepeak was again confirmed to originate from the Ge-Ge correlation, and the corresponding differential pair distribution functions $\Delta_i g(r)$ gave precise second shell information on the Ge-Se-Se correlation. Smaller bond angles of $\sim 90^\circ$ were observed indicating Se dimers interconnecting $\text{Ge}(\text{Se}_{1/2})_4$ tetrahedra. However, due to the large concentration difference between the two measurements, it was not possible to clarify the relation between stiffness transition and structural properties, although previous AXS¹⁹ and neutron-scattering²⁰ data were additionally taken into account. Moreover, the discussion remained on the qualitative level, and even partial structure factors $S_{ij}(Q)$ could hardly be obtained due to small errors in the $\Delta_i S(Q)$ data sets.

Very recently, Inam *et al.*²² carried out *ab initio* molecular dynamics (MD) simulations on the $\text{Ge}_x\text{Se}_{1-x}$ glasses over a wide concentration range of $0.10 \leq x \leq 0.333$, and concluded that the intermediate phase in this glassy system may arise from a competition between a tetrahedral amorphous GeSe_2 and a polymeric amorphous Se. They also pointed out that the system evolves in a nonrandom way or a phase-separation tendency as x changes. This was also confirmed experimentally with x-ray absorption near-edge structure (XANES) experiments near the Ge and Se K edges by Chen *et al.*,²³ which reveal compositional plateaus that coincide with the intermediate phase compositions.

In this study, we have measured AXS in fine concentration steps of $0.02\text{--}0.03$ in the concentration range $0.15 \leq x \leq 0.333$. Some of the experimental results and the qualitative discussion were preliminarily given elsewhere.²⁴ The experimental $\Delta_i S(Q)$ data were analyzed using reverse Monte Carlo (RMC) modeling²⁵⁻²⁷ to obtain $S_{ij}(Q)$ and the corresponding partial pair distribution functions $g_{ij}(r)$ from which detailed three-dimensional atomic configurations across the stiffness transition were obtained. The feasibility of the combination of AXS experiments and RMC modeling was already emphasized by Waseda and co-workers.²⁸

In this paper, the experimental procedure and the data analysis are given in Secs. II and III, respectively. Results of experiment and RMC modeling are presented in Sec. IV. In Sec. V, we discuss the concentration dependence of the atomic structure in glassy $\text{Ge}_x\text{Se}_{1-x}$ in terms of the Phillips-Thorpe rigidity percolation theory.^{1,2} A conclusion is given in the last section.

II. EXPERIMENTAL PROCEDURE

Glassy $\text{Ge}_x\text{Se}_{1-x}$ samples with $x = 0.15, 0.17, 0.20, 0.23, 0.25, 0.28,$ and 0.333 were prepared by quenching the melts after rocking quartz ampoules containing the mixed

compounds with proper concentrations. The purity of the starting elemental materials was 99.999%. In each sample, the melt was homogenized at ~ 1000 °C (~ 60 °C higher than the melting point of Ge) for at least 48 h, and then equilibrated at ~ 50 °C above the liquidus temperature for additional 24 h before the sample was quenched in iced water. The concentration and homogeneity of the samples were examined by measuring Raman-scattering spectra at several different positions of the quenched samples.

The AXS technique utilizes the anomalous change of the atomic form factor of a specific element if the incident x-ray energy is near an absorption edge of the respective element. The complex atomic form factor of an element is given as

$$f(Q, E) = f_0(Q) + f'(E) + if''(E), \quad (1)$$

where f_0 is the usual energy-independent term, and f' and f'' are the real and imaginary parts of the anomalous term, respectively. In general, f is governed by the Q -dependent $f_0(Q)$ in a normal x-ray scattering process, and the anomalous term is negligible. When the incident x-ray energy approaches an absorption edge of a constituent element, however, $f'(E)$ has a large negative minimum and $f''(E)$ shows an abrupt jump near the corresponding absorption edge energies of each element.

One can utilize the difference between two scattering spectra near an absorption edge of the i th element $\Delta_i I$, where one is typically measured at some 10 eV and one at some 100 eV below the absorption edge (E_{near} and E_{far} , respectively). This differential intensity is expressed as

$$\alpha_i \Delta_i I(Q, E_{\text{far}}, E_{\text{near}}) = \Delta_i[\langle f^2 \rangle - \langle f \rangle^2] + \Delta_i[\langle f \rangle^2] \Delta_i S(Q), \quad (2)$$

where α_i is a normalization constant, and $\Delta_i[\]$ indicates the difference of values in the bracket at the energies of E_{far} and E_{near} , close to the absorption edge of the i th element.

The $\Delta_i S(Q)$ functions are given by a linear combination of $S_{ij}(Q)$ as

$$\Delta_i S(Q) = \sum_{i=1}^N \sum_{j=1}^N W_{ij}(Q, E_{\text{far}}, E_{\text{near}}) S_{ij}(Q), \quad (3)$$

where the weighting factors are given by

$$W_{ij}(Q, E_{\text{far}}, E_{\text{near}}) = x_i x_j \frac{\Delta_i[f_i f_j]}{\Delta_i[\langle f \rangle^2]}. \quad (4)$$

It should be noted that compared to $S(Q)$, $\Delta_i S(Q)$ highly enhances the contributions of the i th element related partial structures, and suppresses the other partials.

The AXS measurements were carried out using a standard ω - 2θ diffractometer installed at the beamline BM02 of the European Synchrotron Radiation Facility (ESRF) in Grenoble, France. Details of the experimental setup are given elsewhere.²⁹ X rays generated from a bending magnet source were monochromatized by a Si(111) double-crystal monochromator with a sagittal focusing system for the second crystal. The monochromator was located between two cylindrically bent mirrors made of Si coated by Pt. This x-ray optics provided a small incident x-ray beam size of 0.1 mm in height and 0.3 mm in width, and an energy resolution of

~ 1 eV at an x-ray energy of ~ 10 keV. The energy of the incident x-ray beam was calibrated using the L_{III} absorption edge of an Au foil (11 918 eV) before and after the experiments, and *in situ* using the Ge and Se K edges (11 103 and 12 654 eV, respectively) of the samples during the experiments. The diffraction experiments were performed at two energies (-15 and -200 eV) below the K edge of each element.

III. DATA ANALYSIS

The determination of the anomalous terms $f'(E)$ and $f''(E)$ in $f(Q, E)$ is one of the most difficult processes in the AXS analysis. The f' and f'' values were theoretically calculated at several characteristic K radiation energies by Cromer and Lieberman^{30,31} employing the relativistic dipole approximation method. This Cromer-Lieberman theory was extended over a wide energy range by Brennan and Cowan³² and Sasaki.³³

In the previous AXS papers on Ge-Se glasses,^{21,24,34} Sasaki's values of Ge and Se were used for the AXS data analysis. They are given in Table I. For the GeSe₂ (Ge_{0.333}Se_{0.677}) glass, reliable $S_{ij}(Q)$ data could be obtained employing the NDIS technique.²⁰ Using these $S_{ij}(Q)$ spectra, $\Delta_{\text{Ge}} S(Q)$ and $\Delta_{\text{Se}} S(Q)$ can be calculated by taking x-ray scattering form factors into account. By comparing them with previously obtained experimental $\Delta_{\text{Ge}} S(Q)$ and $\Delta_{\text{Se}} S(Q)$, large overestimates are seen in the amplitude of the oscillations. Thus, it was concluded that the theoretical f' values may be different from those of the real Ge-Se glasses. A discrepancy of more than 10% for f'_{Ge} between theory and experiment was also reported for single-crystal Ge.³⁵

In order to solve these discrepancies, proper corrections were made for f'_{Ge} and f'_{Se} at energies close to the K edges, taking into account neutron-diffraction data on glassy GeSe₂.²⁰ The detailed fitting results are given elsewhere.³⁶ The resultant f' values are given in Table I, and marked by a "c." The differences are $\sim 14\%$ in f'_{Ge} and 3% in f'_{Se} . The corrected f' values near the corresponding absorption edges and the other theoretical values were used for the present analyses of the AXS spectra along the whole x range.

The weighting factors W_{ij} were calculated using these f' and f'' values. For the calculation, the theoretical values of $f_0(Q)$ were taken from literature.³⁷ Circles, squares, and triangles in Fig. 1 show the W_{ij} values of the Ge-Ge, Ge-Se, and Se-Se correlations, respectively, as a function of the Ge concentration x for (a) $\Delta_{\text{Ge}} S(Q)$, (b) $\Delta_{\text{Se}} S(Q)$, and (c) $S(Q)$ at $Q = 20.5 \text{ nm}^{-1}$, which is near the $S(Q)$ maxima of all these

TABLE I. Theoretical (Ref. 33) and corrected (marked by c) f' and f'' values of Ge and Se elements in electron units at energies measured.

Element	Energy (eV)	f'_{Ge}	f''_{Ge}	f'_{Se}	f''_{Se}
Ge	10903	-3.647	0.510	-1.750	0.656
	11088	-6.292	0.494	-1.844	0.635
		-7.194 ^c			
Se	12454	-1.254	3.157	-3.725	0.515
	12639	-1.113	3.084	-6.141	0.500
				-6.310 ^c	

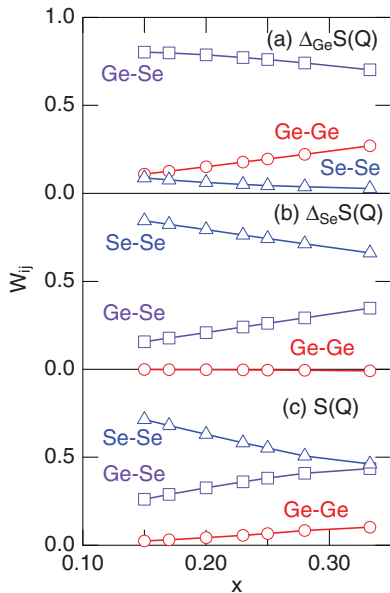


FIG. 1. (Color online) The W_{ij} values of the Ge-Ge (circles), Ge-Se (squares), and Se-Se (triangles) correlations as a function of the Ge concentration x for (a) $\Delta_{\text{Ge}}S(Q)$, (b) $\Delta_{\text{Se}}S(Q)$, and (c) $S(Q)$ at $Q = 20.5 \text{ nm}^{-1}$, near the $S(Q)$ maximum positions of all glasses (Ref. 13).

glasses.¹³ They all change slightly with Q . As expected above, the Se-Se and Ge-Ge contributions are highly suppressed in $\Delta_{\text{Ge}}S(Q)$ and $\Delta_{\text{Se}}S(Q)$, respectively. The Ge-Ge contribution term rapidly decreases with decreasing x , while the Se-Se term increases. The Ge-Se term changes with x , depending on the respective $\Delta_i S(Q)$.

RMC modeling^{25–27} is a useful tool to construct three-dimensional (3D) structural models of disordered materials using experimental diffraction data. In the RMC simulation technique, the atoms of an initial configuration are moved so as to minimize the deviation from experimental structural data, e.g., in this study, $S(Q)$, $\Delta_{\text{Ge}}S(Q)$, and $\Delta_{\text{Se}}S(Q)$, by a standard Metropolis Monte Carlo algorithm.³⁸

The starting configurations were generated by hard-sphere Monte Carlo simulations. They contained 4500 atoms and a simulated box size was chosen to match the number densities of the samples. The constraints for the RMC simulations were applied threefold: shortest atomic distances, the $8 - N$ connectivity, and the bond angle in the $\text{Ge}(\text{Se}_{1/2})_4$ tetrahedra. The choices of the shortest atomic distances were determined to avoid physically unreasonable spikes in $g_{ij}(r)$ in the low r range. The cutoff values were determined to be 0.22, 0.23, and 0.19–0.22 nm for Ge-Ge, Ge-Se, and Se-Se atomic pairs, respectively. The connectivity constraints were adopted by preferring the $8 - N$ rule, i.e., all Ge atoms were likely coordinated to four Se atoms, and all Se atoms to two Ge or Se atoms depending on x . A weak constraint was also applied to the Se-Ge-Se bond angle to avoid unphysically large distortions of the $\text{Ge}(\text{Se}_{1/2})_4$ tetrahedra.

The RMC simulations were performed using the RMC++ program package coded by Gereben *et al.*²⁷ This kind of RMC modeling was successfully applied to SiO_2 and GeO_2 glasses (isovalent compounds of GeSe_2) by Kohara *et al.*^{39,40}

to construct the 3D atomic configurations from a combination of high-energy x-ray and neutron-diffraction data.

IV. RESULTS

Circles in Fig. 2 show the x dependence of (a) $\Delta_{\text{Ge}}S(Q)$, (b) $\Delta_{\text{Se}}S(Q)$, and (c) $S(Q)$. For the $\text{Ge}_{0.333}\text{Se}_{0.667}$ (GeSe_2) glass, the features of $\Delta_{\text{Ge}}S(Q)$ are very different from those of the corresponding $S(Q)$: It has a much larger sharp prepeak at $\sim 10 \text{ nm}^{-1}$. Moreover, there is a large and sharp negative minimum at 20.5 nm^{-1} , where the first peak is located in $S(Q)$. In addition, the second peak in $\Delta_{\text{Ge}}S(Q)$ at approximately $Q = 35 \text{ nm}^{-1}$ has a shoulder at $\sim 25 \text{ nm}^{-1}$, which locates between the first and second peaks in $S(Q)$. On the other hand, $\Delta_{\text{Se}}S(Q)$ of the $\text{Ge}_{0.333}\text{Se}_{0.667}$ glass shows even a minimum at the prepeak position in $S(Q)$ and $\Delta_{\text{Ge}}S(Q)$, and the first peak is much higher than that in $S(Q)$. At higher $Q > 30 \text{ nm}^{-1}$, the spectral shape of $\Delta_{\text{Se}}S(Q)$ closely resembles that of $S(Q)$.

The $\Delta_i S(Q)$ of the $\text{Ge}_{0.333}\text{Se}_{0.667}$ glass were already presented in the pioneering AXS work by Fuoss *et al.*⁴¹ They are displayed in Fig. 2(b) of Ref. 41. Besides the difference in the statistical quality, however, some large discrepancies are observed, i.e., (1) $\Delta_{\text{Ge}}S(Q)$ has no negative drop at the first $S(Q)$ maximum in $S(Q)$ and (2) $\Delta_{\text{Se}}S(Q)$ exhibits a small peak at the prepeak position in $S(Q)$.

With decreasing x , the prepeak at $\sim 10 \text{ nm}^{-1}$ in $\Delta_{\text{Ge}}S(Q)$ broadens and becomes lower in height. However, the prepeak position remains almost unchanged, which is different from the prepeak in $S(Q)$, which shifts toward higher Q values with decreasing x . The sharp negative minimum at $\sim 20 \text{ nm}^{-1}$ gets buried at $x \sim 0.23$. Beyond $Q \sim 25 \text{ nm}^{-1}$, however, no further variations of $\Delta_{\text{Ge}}S(Q)$ are observed over the whole x range, indicating that the SRO around the Ge atoms in $\text{Ge}_x\text{Se}_{1-x}$ glasses does not change drastically with varying x .

As regards the $\Delta_{\text{Se}}S(Q)$ spectra, there is a small minimum at the prepeak position in $S(Q)$, $\sim 10 \text{ nm}^{-1}$, which disappears with decreasing x . The sharp first peak at approximately $Q = 20 \text{ nm}^{-1}$ decreases in height. Finally, besides the magnitude of the prepeak, the shape of $\Delta_{\text{Se}}S(Q)$ at $x = 0.15$ is very similar to that of $S(Q)$. Similar to the $\Delta_{\text{Ge}}S(Q)$ spectra, there is no variation with x above $Q \sim 25 \text{ nm}^{-1}$, indicating that the SRO around the Se atoms in $\text{Ge}_x\text{Se}_{1-x}$ glasses does also not change drastically with x . The general features in $\Delta_{\text{Ge}}S(Q)$ and $\Delta_{\text{Se}}S(Q)$ at $x = 0.25$ and 0.167 measured previously by Armand *et al.*¹⁹ are very similar to the present results, although small differences are seen, due probably to the difference of the used incident energies. Also, the statistical quality is considerably better in the present work.

An interesting feature was observed from a detailed inspection of the spectra: There is a small shoulder in $\Delta_{\text{Se}}S(Q)$ at $Q \sim 15 \text{ nm}^{-1}$. By taking the weighting factors of $S_{ij}(Q)$ s in $\Delta_i S(Q)$ into account, this shoulder can be interpreted as resulting from the presence of Se-Se intermediate-range correlations around this Q position. A similar shoulder in the prepeak region in $\Delta_{\text{Se}}S(Q)$ was found previously in our AXS study on As_2Se_3 glass.⁴²

The solid curves in Fig. 2 indicate the best fits of the RMC modeling. All of the fit curves coincide well with the corresponding experimental data. Small discrepancies are seen

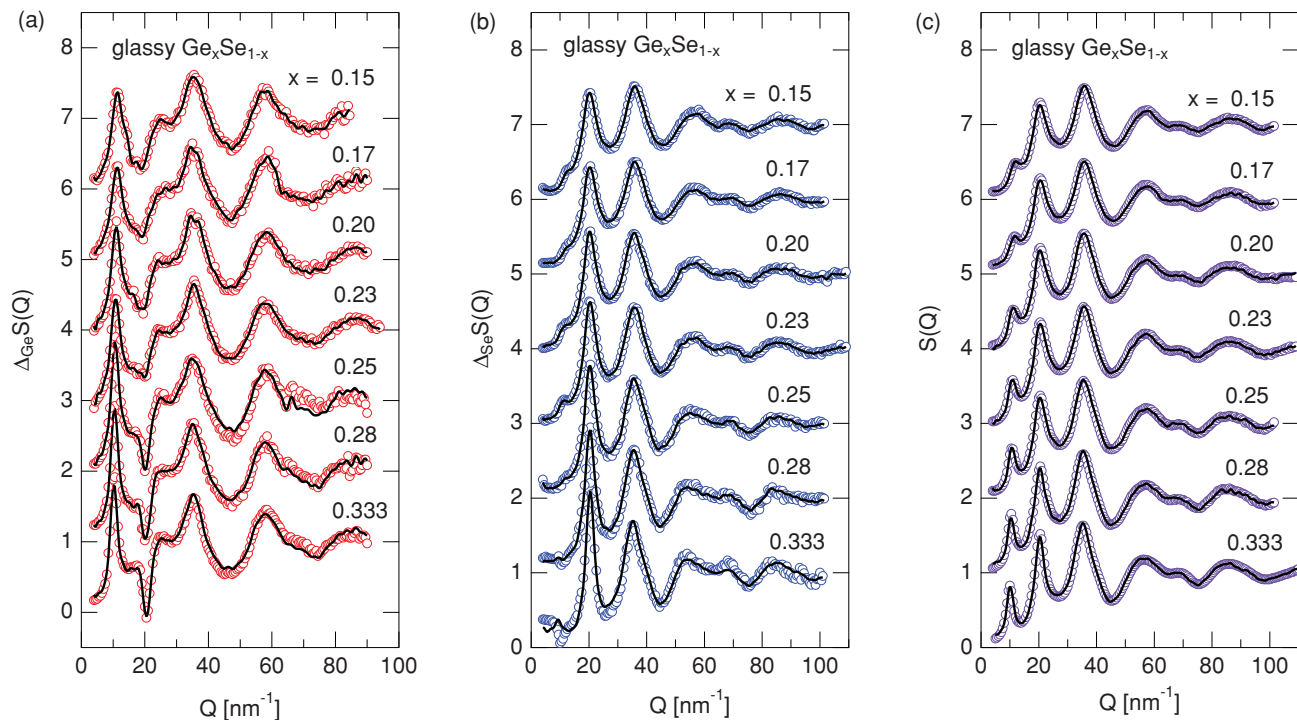


FIG. 2. (Color online) Circles are the x dependence of (a) $\Delta_{\text{Ge}}S(Q)$, (b) $\Delta_{\text{Se}}S(Q)$, and (c) $S(Q)$. The solid curves indicate the best fits of the RMC modeling. The data are shifted each other by 1.

only in $\Delta_{\text{Ge}}S(Q)$ in the high Q range, where the errors are very large due to the low Ge concentration.

Figures 3(a)–3(c) show $S_{\text{GeGe}}(Q)$, $S_{\text{GeSe}}(Q)$, and $S_{\text{SeSe}}(Q)$, respectively, obtained from the RMC modeling. For the $\text{Ge}_{0.333}\text{Se}_{0.667}$ glass, a sharp peak is seen in $\Delta_{\text{GeGe}}(Q)$ at the

prepeak position in $S(Q)$ of $\sim 10 \text{ nm}^{-1}$ with a height of ~ 2.5 , which is much larger than that in $S(Q)$. The present result is very similar to the NDIS finding by Petri *et al.*,²⁰ which was discussed elsewhere.³⁶ The prepeak height changes with decreasing x . Even at $x = 0.15$, however, it is ~ 2 , still higher

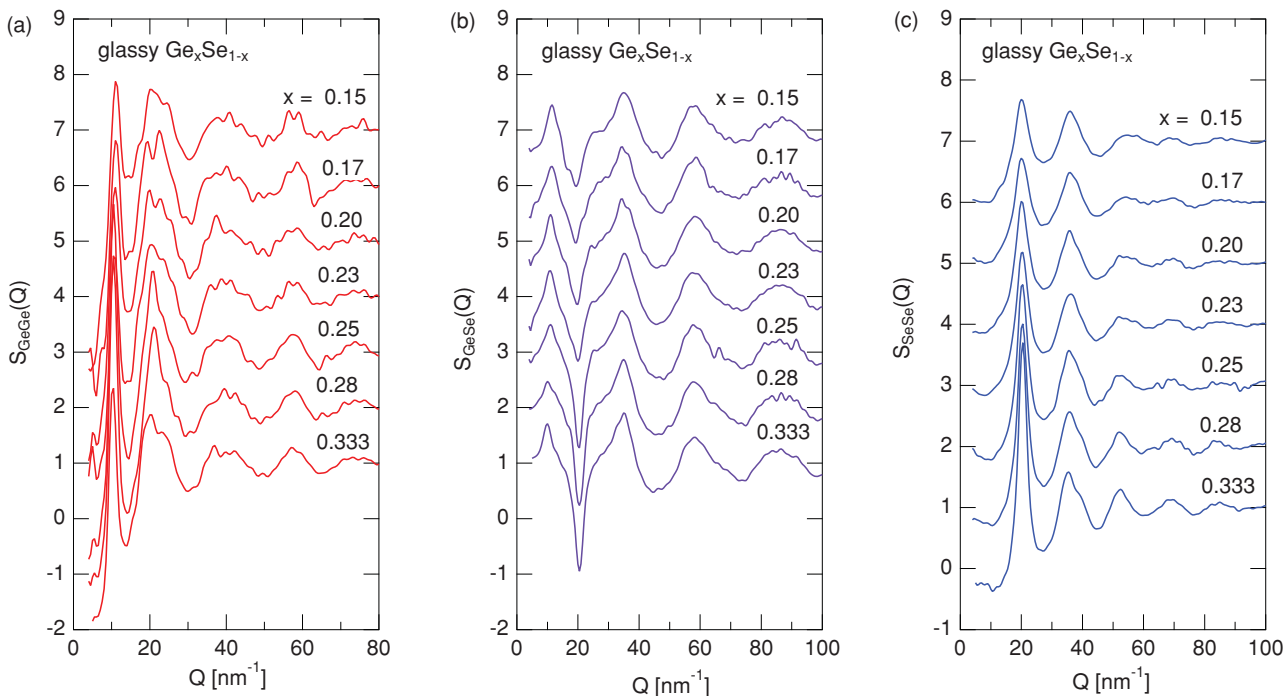


FIG. 3. (Color online) (a) $S_{\text{GeGe}}(Q)$, (b) $S_{\text{GeSe}}(Q)$, and (c) $S_{\text{SeSe}}(Q)$ of $\text{Ge}_x\text{Se}_{1-x}$ glasses obtained from the RMC modeling. The data are shifted each other by 1.

than the height of the first peak at $\sim 20 \text{ nm}^{-1}$. Moreover, prepeak position and width do not vary with x .

The prepeak features in $S_{\text{GeGe}}(Q)$ are very different from those in $S(Q)$, where with decreasing x , the prepeak rapidly decreases in height and shifts toward higher Q values.^{13,15} Thus, it is concluded that the origin of the prepeak in $S(Q)$ is not limited to the Ge-Ge correlations, but may include other contributions from Ge-Se and Se-Se correlations, as was already suspected earlier.¹³

At $Q > \sim 15 \text{ nm}^{-1}$, beyond the first minimum in $S_{\text{GeGe}}(Q)$, no drastic changes are seen with decreasing x , suggesting that the Ge-Ge local structures, or the connections between the $\text{Ge}(\text{Se}_{1/2})_4$ tetrahedra, do not change considerably.

In the $S_{\text{GeSe}}(Q)$ spectrum of the $\text{Ge}_{0.333}\text{Se}_{0.667}$ glass, there is also a peak observed at the prepeak position of $\sim 10 \text{ nm}^{-1}$. Its Q position remains almost unchanged with decreasing x . Thus, the contribution of the Ge-Se correlation must be taken into account to understand the origin of the prepeak in $S(Q)$ for the $\text{Ge}_x\text{Se}_{1-x}$ glasses. A steep and negative hump is observed at the first peak position in $S(Q)$, which becomes shallower and broader with decreasing x . At $Q \geq 23 \text{ nm}^{-1}$, $S_{\text{GeSe}}(Q)$ is slightly damped in amplitude with decreasing x .

In the $S_{\text{SeSe}}(Q)$ spectrum of the $\text{Ge}_{0.333}\text{Se}_{0.667}$ glass, there is no indication of a peak at the prepeak positions as in the other $S_{ij}(Q)$ s. Even a small hump is seen at all concentrations. However, a small shoulder at the low Q side of the first peak at approximately $Q = 15 \text{ nm}^{-1}$ grows up when x is decreased. In order to exhibit this preshoulder in detail, the $S_{\text{SeSe}}(Q)$ spectra are depicted in Fig. 4 on an enlarged scale below the first peak region. The spectra were fitted using two pseudo-Voigt functions, i.e., a linear combination of Gaussian and Lorentzian curves, and the obtained preshoulder contributions are shown by dashed curves in this figure. At $x = 0.15$, a clear shoulder is seen at $\sim 14 \text{ nm}^{-1}$, which is above the prepeak positions in $S_{\text{GeGe}}(Q)$, $S_{\text{GeSe}}(Q)$, and $S(Q)$ of $\sim 11.5 \text{ nm}^{-1}$. With increasing x , the preshoulder position shifts toward higher Q values. At $x = 0.333$, the fit failed and the preshoulder may have disappeared, or merged into the large first peak. It should be noted that since the Se-Se correlation dominates in $S(Q)$ as shown in Fig. 1, this shoulder may have a large contribution to the shape of the prepeak in the $\text{Ge}_x\text{Se}_{1-x}$ glasses, in particular in the low x region.

The first peak in $S_{\text{SeSe}}(Q)$ of $\text{Ge}_{0.333}\text{Se}_{0.667}$ glass has a large height of ~ 3.5 . The following oscillations also show large amplitudes. These oscillations become damped with decreasing x , suggesting the inclusion of different Se-Se correlations in this glassy system in the low x range.

Figures 5(a)–5(c) show $g_{\text{GeGe}}(r)$, $g_{\text{GeSe}}(r)$, and $g_{\text{SeSe}}(r)$, respectively, obtained from the RMC modeling. In the $g_{\text{GeGe}}(r)$ spectrum of $\text{Ge}_{0.333}\text{Se}_{0.667}$ glass, a small peak is observed at $r = 0.23 \text{ nm}$. Petri *et al.*²⁰ discussed the existence of such homopolar wrong bonds at $x = 0.333$. The wrong bonds seem to disappear in the intermediate and floppy ranges $x \leq 0.26$. Since such sharp peaks are sometimes visible close to cutoff distances in the RMC analysis, however, the details of the wrong bonds should not be discussed within the present analysis.

The main peak in $g_{\text{GeGe}}(r)$ of $\text{Ge}_{0.333}\text{Se}_{0.667}$ glass is large (~ 3.5), indicating connections of the $\text{Ge}(\text{Se}_{1/2})_4$ tetrahedra. Since the peak width is rather broad compared to the Si-Si

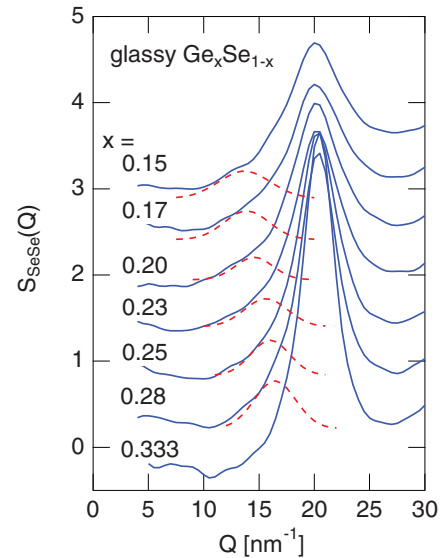


FIG. 4. (Color online) $S_{\text{SeSe}}(Q)$ spectra in an enlarged scale around the first peak region. The preshoulder contributions obtained from two pseudo-Voigt fits are shown by dashed curves. The data are shifted each other by 0.5.

correlation in SiO_2 glass,⁴⁰ the connections between the $\text{Ge}(\text{Se}_{1/2})_4$ tetrahedra in $\text{Ge}_{0.333}\text{Se}_{0.667}$ glass may be distorted, which may originate from some edge-sharing connections between the tetrahedra. With decreasing x , the height of first peak of $g_{\text{GeGe}}(r)$ is slightly diminishing. Beyond the main peak, the statistics of the spectra is relatively poor due to the small Ge concentrations.

In the $g_{\text{GeSe}}(r)$ spectrum of the $\text{Ge}_{0.333}\text{Se}_{0.667}$ glass, a large and narrow first peak is seen at $r \sim 0.235 \text{ nm}$ with a height of ~ 20 , indicating strong Ge-Se covalent bonds. The second largest peak is observed at $r \sim 0.57 \text{ nm}$, which represents the correlation between Ge and Se in the neighboring tetrahedra.

With decreasing x , the peak height of the main peak remains almost unchanged, as expected due to the strong Ge-Se covalent bonds. Between the first and second peaks, a peak at $r \sim 0.36 \text{ nm}$ grows up with increasing x , indicating Se atoms which are attached to the $\text{Ge}(\text{Se}_{1/2})_4$ tetrahedra, i.e., the Ge-(Se)-Se connections.

In the $g_{\text{SeSe}}(r)$ spectrum of the $\text{Ge}_{0.333}\text{Se}_{0.667}$ glass, a small peak is observed at $r \sim 0.22 \text{ nm}$, indicating again the so-called wrong homopolar bonds discussed by Petri *et al.*²⁰ With decreasing x , the number of the Se-Se bonds increases due to the extra Se atoms. The main peak of $g_{\text{SeSe}}(r)$ at $x = 0.333$ locates at $r \sim 0.39 \text{ nm}$ with a large height of ~ 3.5 , originating from Se-(Ge)-Se correlations in the $\text{Ge}(\text{Se}_{1/2})_4$ tetrahedra. With decreasing x , the main peak height diminishes due to the decreasing number of $\text{Ge}(\text{Se}_{1/2})_4$ tetrahedra.

Atomic configurations of glassy $\text{Ge}_x\text{Se}_{1-x}$ obtained by the RMC modeling are illustrated in Fig. 6 at selected x values of (a) $x = 0.333$, (b) 0.25, (c) 0.20, and (d) 0.15. The tetrahedra indicate the $\text{Ge}(\text{Se}_{1/2})_4$ units and the bars are the Se-Se bonds, which are both defined by the atomic distances below 0.26 nm. At $x = 0.333$, the $\text{Ge}(\text{Se}_{1/2})_4$ tetrahedra are mainly connected by corner sharing, while a small number of tetrahedra are connected by edge sharing. It should be

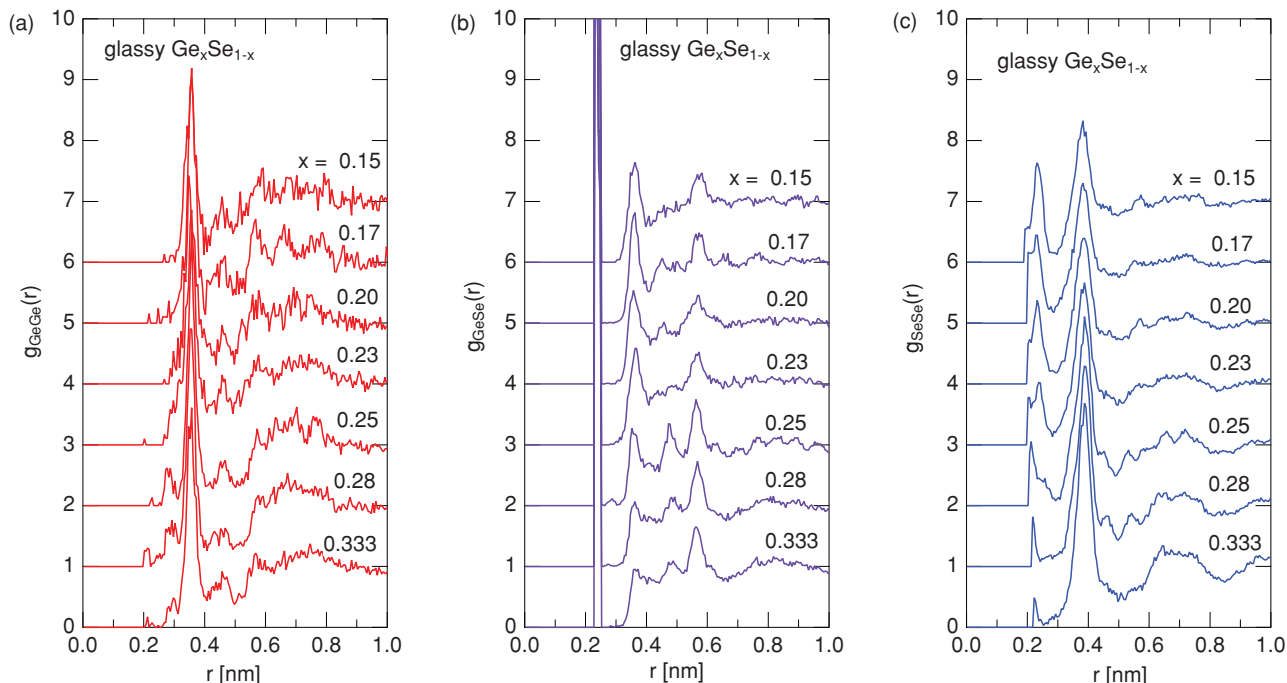


FIG. 5. (Color online) (a) $g_{\text{GeGe}}(r)$, (b) $g_{\text{GeSe}}(r)$, and (c) $g_{\text{SeSe}}(r)$ of $\text{Ge}_x\text{Se}_{1-x}$ glasses obtained from the RMC modeling. The data are shifted each other by 1.

noted that the Se-Se bonds seen in this composition are mainly due to the large distortion of the tetrahedra, and not by the individual Se-Se bonds outside of the tetrahedra. Thus, the short Se-Se correlations seen in the $g_{\text{SeSe}}(r)$ in Fig. 5(c) are not topologically wrong homopolar bonds. Individual Se-Se bonds are seen at $x = 0.25$ and their number increases with decreasing x . Even at $x = 0.15$, some corner- and edge-sharing connections of the $\text{Ge}(\text{Se}_{1/2})_4$ tetrahedra can still be observed in Fig. 6(d).

V. DISCUSSION

A. Comparison to *ab initio* MD simulation

The present AXS results and the RMC modeling of the $\text{Ge}_{0.333}\text{Se}_{0.667}$ glass were already discussed in a previous paper.³⁶ There, the data were compared to $S_{ij}(Q)$ data obtained from NDIS by Petri *et al.*²⁰ and to *ab initio* MD simulations by Massobrio *et al.*⁴³ It was found that the agreement is excellent for the Ge-Se and Se-Se atomic correlations, and acceptable for the Ge-Ge correlation. In this paper, we compare our data from the $\text{Ge}_{0.20}\text{Se}_{0.80}$ glass to results of an *ab initio* MD simulation by Massobrio *et al.*⁴⁴ This composition corresponds to the onset point of the stiffness transition of the Boolchand's criterion.

Figure 7(a) shows the $S_{ij}(Q)$ spectra obtained from the present AXS measurements and the *ab initio* MD simulations,⁴⁴ given by thick and thin solid curves, respectively. The overall features of the spectra exhibit good agreements, in particular in the $S_{\text{SeSe}}(Q)$ and $S_{\text{GeSe}}(Q)$ spectra. The smaller Ge concentration in $\text{Ge}_{0.20}\text{Se}_{0.80}$ as compared to the other composition results in considerably smaller values for the corresponding weighting factors as seen in Fig. 1. This causes large errors in the corresponding $S_{\text{GeGe}}(Q)$ as compared to the data from the other concentrations. The low

Ge concentration also affects the theoretical calculation as seen as large errors in the corresponding functions at the top of Fig. 7(a). A discrepancy between the theory and experiment is visible in the prepeak shape, which may be due to the limited system size of the *ab initio* MD simulation. Moreover, the oscillation in the theoretical $S_{\text{GeGe}}(Q)$ beyond the third peak is shifted to lower Q values as compared to the experimental data.

Figure 7(b) shows the $g_{ij}(r)$ spectra of $\text{Ge}_{0.20}\text{Se}_{0.80}$ obtained from the present AXS measurements and the *ab initio* MD simulation,⁴⁴ given by thick and thin curves, respectively. Again, the overall features of the spectra exhibit good agreement, in particular for the $g_{\text{SeSe}}(r)$ and $g_{\text{GeSe}}(r)$ cases. The first peak in $g_{\text{SeSe}}(r)$ of the theoretical data at ~ 2.1 nm is sharper and larger than that in the experimental $g_{\text{SeSe}}(r)$. However, the coordination number, i.e., the area under the peak, is similar. The so-called wrong homopolar Ge-Ge bonds are hardly seen in the $g_{\text{GeGe}}(r)$ spectra of both curves. The largest disagreement is again observed between the first peaks of the Ge-Ge correlation. In the simulation, two peaks are seen and the larger one is broader and shifted toward larger r values as compared to the single and sharp experimental peak.

Thus, the agreement of the $S_{ij}(Q)$ spectra at $x = 0.20$ obtained from the present AXS measurement and the *ab initio* MD simulation is excellent in the Ge-Se and Se-Se atomic correlations, and acceptable in the Ge-Ge correlation.

B. Intermediate-range order: Prepeak

The prepeak indicates the existence of intermediate-range correlations. As discussed by Petri *et al.*,²⁰ the prepeak in $\text{Ge}_{0.333}\text{Se}_{0.667}$ glass located at ~ 10 nm⁻¹ originates from Ge-Ge correlations. However, a contribution from the Ge-Se

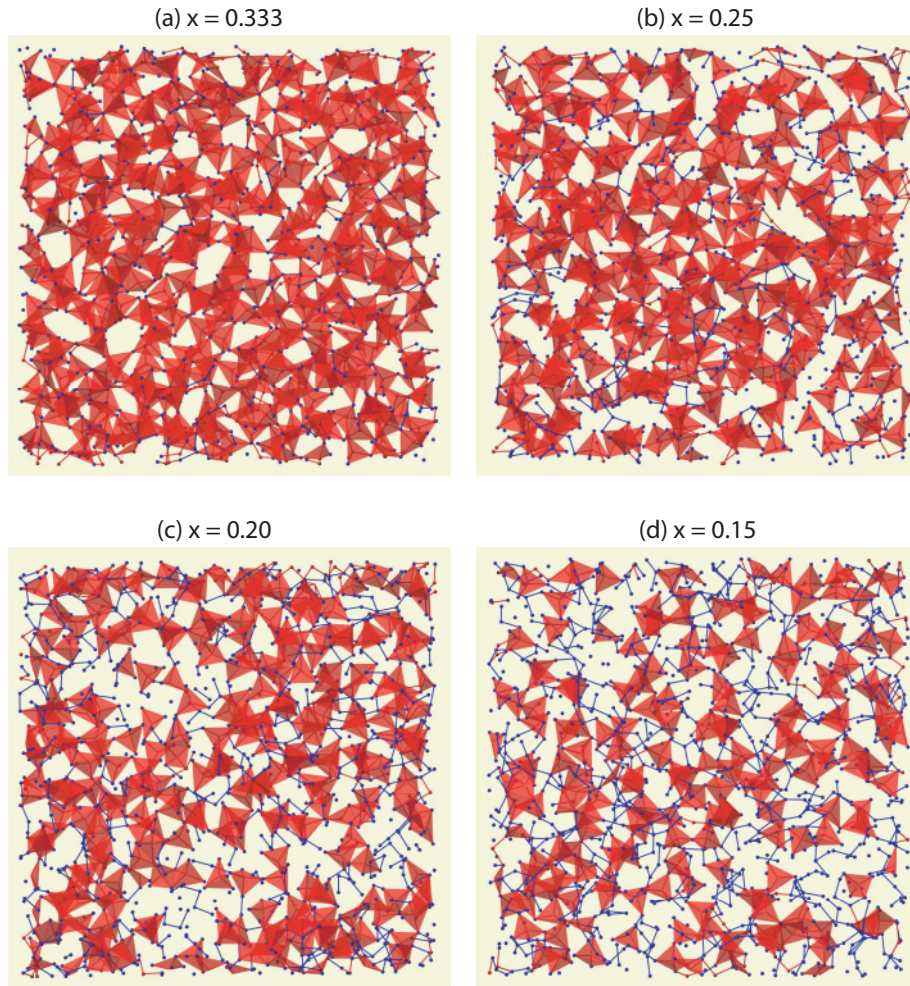


FIG. 6. (Color online) Atomic configurations of glassy $\text{Ge}_x\text{Se}_{1-x}$ obtained by RMC modeling at selected x values: (a) $x = 0.333$, (b) 0.25, (c) 0.20, and (d) 0.15. The tetrahedra indicate the $\text{Ge}(\text{Se}_{1/2})_4$ units and the bars are Se-Se bonds, which are both defined by the atomic distances below 0.26 nm.

correlations cannot be neglected as was pointed out by Massobrio *et al.*⁴⁴ The present AXS with the RMC modeling confirmed these conclusions as shown in Fig. 3.

Figure 8 shows the x dependence of the prepeak or preshoulder positions Q_p observed in $S_{\text{GeGe}}(Q)$, $S_{\text{GeSe}}(Q)$, and $S_{\text{SeSe}}(Q)$, given as circles, squares, and triangles, respectively, together with those in $S(Q)$ taken from a previous paper,¹³ indicated by the solid curve. The Q_p position in $S_{\text{GeGe}}(Q)$ shifts very slightly and linearly toward higher Q values with decreasing x as shown by the dashed line. No anomalies are found in the stiffness transition composition range of Boolchand's criterion^{5,6} $x = 0.26$ – 0.20 . A slightly larger shift is observed in the Q_p position in $S_{\text{GeSe}}(Q)$, and again it seems to show no effect related to the stiffness transition.

On the other hand, a clear decrease from ~ 16 to 14 nm^{-1} is found for the Q_p position in $S_{\text{SeSe}}(Q)$ with decreasing x , where the largest shift occurs exactly in the *intermediate phase* composition range. Thus, the structural change related to the stiffness transition occurs in the Se-Se intermediate-range structure. The contribution of the Se-Se correlations to the prepeak in $\text{Ge}_x\text{Se}_{1-x}$ glasses was already predicted from a detailed analysis of the $S(Q)$ spectra,¹³ where it was found that the overall features of the $Q_p(x)$ function are similar to the present finding. There, we also observed a sharp shift of the Q_p positions in $S_{\text{SeSe}}(Q)$. However, we found that $S_{\text{GeSe}}(Q)$ has also a considerable contribution to the prepeak.

The origin of the prepeak in $S(Q)$ of the $\text{Ge}_x\text{Se}_{1-x}$ glasses can now be discussed in detail using the present AXS results, by taking the weighting factors and the prepeak heights in the $S_{ij}(Q)$ functions into account. At $x = 0.333$, the contributions of the Ge-Ge and Ge-Se correlations to $S(Q)$ are $\sim 10.3\%$ and $\sim 43.6\%$, respectively as can be inferred from Fig. 1(c). This indicates that the Ge-Ge contribution to the prepeak height in $S(Q)$ is only $\sim 25\%$, while the remaining intensity comes from the Ge-Se contribution. With decreasing x , the weighting factor of the Ge-Ge correlation decreases, and the Ge-Se contribution dominates the prepeak features in $S(Q)$. In the floppy regime at $x \leq 0.20$, the preshoulder in $S_{\text{SeSe}}(Q)$ shifts toward lower Q values, and starts to contribute to the prepeak in $S(Q)$, resulting in a deviation from the linear x dependence of the prepeak positions in $S(Q)$ towards higher Q values.

C. Local structures around the Ge and Se atoms

In order to discuss the coordination numbers and the bond angles, the atomic bonds were defined as the atomic distances below 0.26 nm, where the first and second coordination shells are clearly separated as can be seen in the $g_{ij}(r)$ spectra in Fig. 5.

Figure 9 shows the averaged partial coordination numbers N_{ij} , i.e., mean number of j th atoms surrounding the i th atom. The values for Ge and Se atoms surrounding Ge are indicated

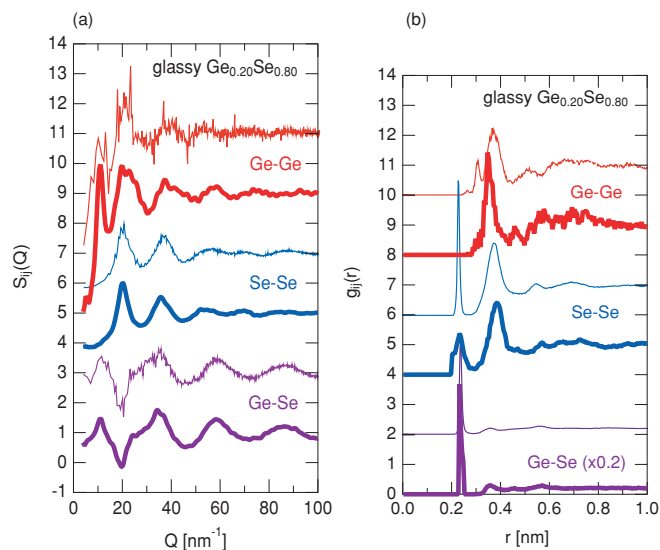


FIG. 7. (Color online) Comparison of the present AXS results (thick curves) with the *ab initio* MD simulation (Ref. 44) (thin curves) in (a) $S_{ij}(Q)$ and (b) $g_{ij}(r)$ of $\text{Ge}_{0.20}\text{Se}_{0.80}$ glass. From top to bottom, the Ge-Ge, Se-Se, and Ge-Se partials are given. The $g_{\text{GeSe}}(r)$ spectra are reduced by 0.2 in the vertical axes. The data are shifted each other by 2.

as Ge-Ge and Ge-Se in the figure and given by open and solid circles, respectively. Similarly, those around Se (Se-Ge and Se-Se) are given by solid and open triangles, respectively. The lines indicate the ideal partial coordination numbers predicting the chemically ordered continuous-random-network model.⁴⁵

At $x = 0.333$, the Ge atoms are mostly surrounded by four Se atoms and the Se atoms by two Ge atoms. The average numbers of the so-called wrong bonds (homopolar bonds) N_{GeGe} and N_{SeSe} are very small values of 0.013 and 0.176 for the Ge-Ge and Se-Se bonds, respectively. N_{GeGe} is smaller than the corresponding value of the *ab initio* MD simulation result⁴³ of 0.07 ± 0.04 and the experimental value of the neutron diffraction²⁰ of 0.25 ± 0.05 . On the other hand, N_{SeSe}

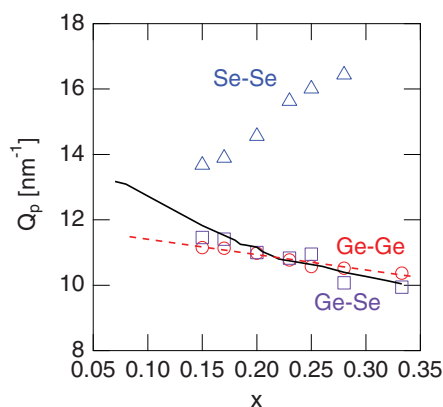


FIG. 8. (Color online) The Q positions of the prepeaks or preshoulders in the Ge-Ge (circles), Ge-Se (squares), and Se-Se (triangles) partial structure factors as a function of x . The solid curve indicates the prepeak positions in $S(Q)$ taken from the previous paper (Ref. 13), and the dashed line is a guide for the eyes for the prepeak positions in $S_{\text{GeGe}}(Q)$.

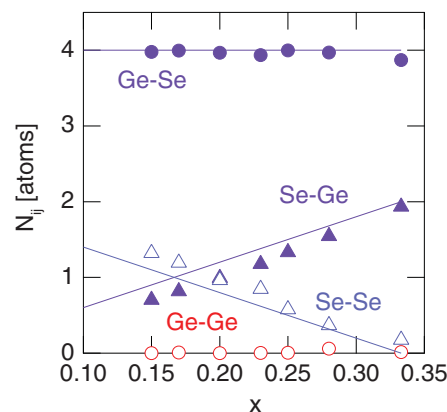


FIG. 9. (Color online) The averaged partial coordination numbers N_{ij} of Ge and Se atoms around Ge (Ge-Ge and Ge-Se, open and solid circles), and those around Se (Se-Ge and Se-Se, solid and open triangles), respectively. The lines indicate the ideal partial coordination numbers assuming the chemically ordered continuous-random-network model (Ref. 45).

is similar to the neutron result of 0.20 ± 0.05 , and slightly smaller than the theoretical value of 0.27 ± 0.03 .

If the wrong homopolar bonds are induced by simple bond switching from Ge-Se to Ge-Ge and Se-Se, the N_{SeSe} value should be twice as large as N_{GeGe} . However, the ratio $N_{\text{SeSe}}/N_{\text{GeGe}}$ is much more than 10. From a detailed inspection of the atomic configurations in Fig. 6(a), it can be inferred that besides the real wrong bonds of Se-Se dimers, there are also short Se-Se bonds belonging to the short edges of highly deformed $\text{Ge}(\text{Se}_{1/2})_4$ tetrahedra.

With decreasing x , N_{SeGe} decreases and N_{SeSe} increases, mostly following the prediction of the chemically ordered continuous-random-network model.⁴⁵ Small deviations from the model are seen in the N_{ij} values around the Se atoms in the *intermediate phase* and floppy regions $x \leq 0.26$, indicating that the Se-Se bonds are more preferred than the Se-Ge bonds in these concentration ranges.

The total coordination numbers around the Ge and Se atoms are 4.00 ± 0.05 and 2.00 ± 0.15 , respectively, along the concentration range $0.15 \leq x \leq 0.333$, indicating that the 8 - N rule is more or less applicable for the $\text{Ge}_x\text{Se}_{1-x}$ glasses in this concentration range.

In Fig. 10(a), the Ge-Se-Ge bond angle distribution for the $\text{Ge}_x\text{Se}_{1-x}$ glasses are shown. At $x = 0.333$, two peaks are seen centered at $\sim 79^\circ$ and $\sim 97^\circ$, respectively. From the NDIS experiment, these values were estimated to be 80° and 98° by Salmon,⁴⁶ as given by the down arrows at the bottom of Fig. 10(a), which is in excellent agreement with the present AXS result. The smaller and larger peaks in the Ge-Se-Ge bond angles are assigned to the edge- and corner-sharing $\text{Ge}(\text{Se}_{1/2})_4$ tetrahedra, respectively. On the other hand, larger values of 83° and 102° are obtained by the *ab initio* MD simulation,⁴³ as indicated by the up arrows at the bottom of Fig. 10(a).

A clear analysis of the Ge-Se-Ge bond angle distribution dependence on x is difficult because the statistical quality of the data worsens due to the decreasing Ge content. However, the main features of the distribution with a broad peak centered at $\sim 98^\circ$ remains more or less unchanged. The theoretical results⁴⁴ at $x = 0.20$ are again indicated by the up arrows.

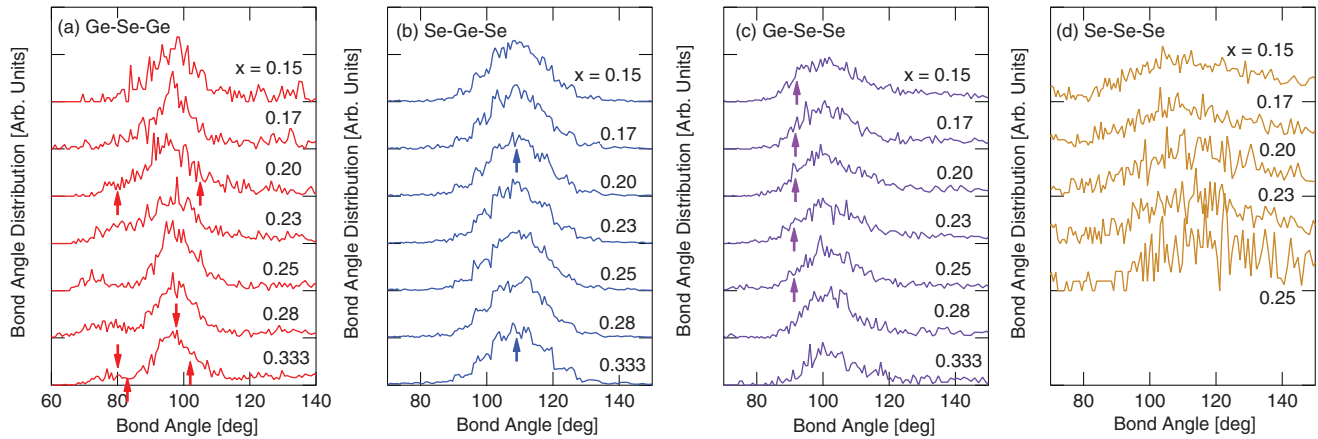


FIG. 10. (Color online) The bond angle distributions of (a) Ge-Se-Ge, (b) Se-Ge-Se, (c) Ge-Se-Se, and (d) Se-Se-Se. The down arrows in (a) represent the peak positions for GeSe₂ ($x = 0.333$) obtained from the NDIS measurement (Ref. 46), and the up arrows in (a) and (b) indicate those for GeSe₂ ($x = 0.333$) and GeSe₄ ($x = 0.20$) obtained from the *ab initio* MD simulations (Refs. 43 and 44), and those in (c) show additional distributions of the Ge-Se-Se bond angles near the right angle in the low x region.

They are, however, much higher than the findings from the experiment.

Figure 10(b) shows the Se-Ge-Se bond angle distributions, and the arrows indicate the peak positions of the *ab initio* MD simulation results.^{43,44} Since a weak constraint was applied to avoid too large distortions of the Ge(Se_{1/2})₄ tetrahedra, rather symmetrical peaks are observed in the Se-Ge-Se bond angle distributions centered at 109°, reflecting the predominant fourfold coordination environment around the Ge atoms. As clearly seen in the figure, the Ge(Se_{1/2})₄ tetrahedral configurations remain unchanged along the whole x range.

Figure 10(c) shows the Ge-Se-Se bond angle distributions. This angle is assigned to represent the connection between a Ge atom at a tetrahedral center and an additional Se atom attached to a Se atom at the tetrahedron corner. At $x = 0.333$, they form the so-called wrong bonds, and the main peak is located at $\sim 100^\circ$. With decreasing x , the spectral features of the distributions remains basically unchanged. In the stiffness transition region, however, a shoulder grows up at $\sim 90^\circ$, as indicated by the up arrows in Fig. 10(c). The existence of such a small bond angle was already pointed out in a previous AXS paper²¹ with a preliminary analysis of $\Delta_i S(Q)$ in the stiffness transition region, and an *ab initio* MD simulation on liquid Ge_{0.20}Se_{0.80}.⁴⁷

Figure 10(d) shows the Se-Se-Se bond angle distributions. Owing to the small numbers of the Se_{*n*} chains ($n \geq 3$), the data at $x = 0.333$ and 0.28 are omitted from the figure. Along the whole x range, the distributions show a broad peak centered at $\sim 105^\circ$ – 110° , similar to the Se-Se-Se bond angle of 103° – 105° in glassy⁴⁸ and crystalline⁴⁹ trigonal Se.

D. Intermediate-range order: Connections between tetrahedra

It was believed for a long time that the prepeak located at $Q_p \sim 10 \text{ nm}^{-1}$ in GeSe₂ glass represents the existence of intermediate-range order with a correlation length of approximately $r = 2\pi/Q_p \sim 0.63 \text{ nm}$ in real space. However, there is no spatial indication for the correlation in real space at that length scale as shown in, e.g., the $g_{ij}(r)$ spectra in Fig. 5.

Instead, we speculated about another origin in our previous papers.^{13,21} The $S_{\text{GeGe}}(Q)$ of GeSe₂ glass closely resembles the $S(Q)$ of pure amorphous Ge when the Q value is appropriately scaled with the ratio of the Ge-Ge distances in amorphous Ge (0.246 nm) to that in GeSe₂ glass (0.357 nm). Then, the prepeak in $S_{\text{GeGe}}(Q)$ of GeSe₂ glass corresponds to the first peak in $S(Q)$ of amorphous Ge.⁵⁰ In other words, the Ge sublattice in GeSe₂ glass forms a fourfold coordinated amorphous-Ge-like configuration.

In order to observe different types of connections between the tetrahedra, the fractions of the Se atoms belonging to Se_{*n*} chains are given in Fig. 11. They mostly correspond to the Se chain length connecting two Ge atoms centered at the tetrahedra if dangling bonds and connection of highly distorted tetrahedra are neglected.

At $x = 0.333$, where most of the tetrahedra are connected by corner or edge sharing, the single Se atoms (monomer) dominate, and the existence of $\sim 10\%$ of Se₂ dimers originates

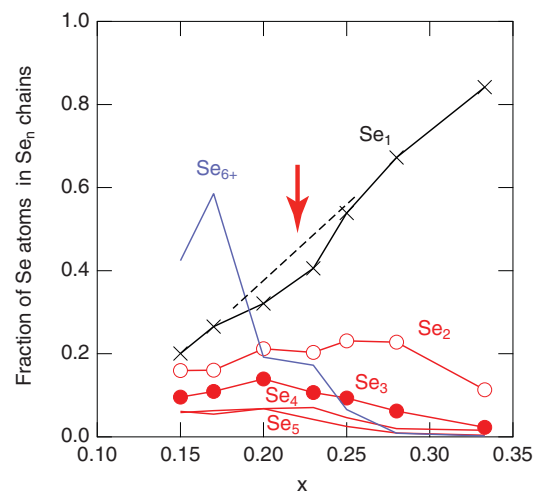


FIG. 11. (Color online) The fractions of the number of Se atoms belonging to the Se_{*n*} chains. The dashed line is a guide for the eyes.

from wrong bonds or highly distorted tetrahedra as discussed in Sec. VC.

With decreasing x in the stressed-rigid region $0.333 \geq x \geq 0.26$, the fraction of the Se_1 monomer decreases, and those of the Se_2 dimer and the Se_3 trimer increase as expected. In the unstressed-rigid or *intermediate phase* region $0.26 \geq x \geq 0.20$, the fraction of the Se_1 monomer largely decreases, as indicated by the thick arrow. On the other hand, the fraction of the Se_2 dimer remains almost constant. Thus, the decrease of the Se_1 monomer is compensated by the formation of longer Se_n ($n \geq 3$) chains.

With a further decrease of x in the floppy region $x \leq 0.20$, the fractions of the Se_2 dimers as well as the Se_3 trimers gradually decrease, and those of the Se_4 and Se_5 remain constant. On the contrary, the fraction of the Se_n long chains with more than six Se atoms rapidly increases. It should be noted that the fraction of the Se_1 monomer connections from the corner- and edge-sharing tetrahedra is still larger than that of the Se_2 dimer connections. From Raman-scattering and infrared spectroscopic measurements,⁵¹ theoretical analysis for the vibration properties,⁵² and also intuitively from the statistical average, it was supposed that at $x = 0.20$, the $\text{Ge}(\text{Se}_{1/2})_4$ tetrahedra are preferred to be connected by Se_2 dimers. However, the present result reveals that longer chains and monomers are preferred for tetrahedral connections rather than Se_2 dimers.

Information from Raman scattering is very helpful to understand the x dependence of the IRO. Selvanathan *et al.*⁵³ analyzed the area under the Raman-scattering spectra of A_1 , A_1^c , and A_{Se} modes in isovalent $\text{Si}_x\text{Se}_{1-x}$ glasses, which respectively correspond to populations of the corner-, edge-sharing, and Se chain connected tetrahedra (S_{CS} , S_{ES} , and S_{Se}). The corner- and edge-sharing tetrahedra exist over a wide concentration range down to $x \leq 0.07$, and their populations seem to have no anomalies at the stiffness transition concentrations. However, the authors pointed out that the mode peaks characteristic for Se chains are asymmetric, and were analyzed using two Gaussians. From a detailed analysis, they assigned the sharp high-frequency contribution as the stretching mode of Se_2 , and the broad low-frequency part as the Se_n ($n \geq 3$) long chain mode. As a peculiar result associated with the stiffness transition, it must be emphasized that the Se_2 mode area vanishes at $x < 0.19$. Similar experimental data were obtained for $\text{Ge}_x\text{Se}_{1-x}$ glasses.^{5,6} However, to the best of our knowledge, no detailed analysis has yet been performed.

There are two large discrepancies between the Raman-scattering data on the $\text{Si}_x\text{Se}_{1-x}$ glasses and the present AXS results on the $\text{Ge}_x\text{Se}_{1-x}$ glasses. First, the ratio of the corner- and edge-sharing connections in glassy $\text{Ge}_{0.333}\text{Se}_{0.667}$ is different from the Raman-scattering results on the SiSe_2 glass, where $\sim 2/3$ of the tetrahedral connections are formed by edge sharing, while only $\sim 10\%$ are edge sharing in the $\text{Ge}_{0.333}\text{Se}_{0.667}$ glass. The Raman-scattering data on the $\text{Ge}_{0.333}\text{Se}_{0.667}$ glass qualitatively support the present AXS result. The A_1^c mode intensity is much smaller than the A_1 mode intensity, as shown in Fig. 2 of Ref. 6. This large difference may be due to the different cations Si and Ge, although they are isovalent, and the Si atoms may rather prefer to form the edge-sharing connections between the $\text{Si}(\text{Se}_{1/2})_4$ tetrahedra.

Second, the Se_2 dimer fraction does not vanish in the floppy regime, although it gradually decreases down to less than 20%. Since the fractions of the longer Se_n ($n \geq 3$) connections rapidly increase with decreasing x in the floppy region, the Raman-scattering peak of the Se_2 dimers may be hidden under the large peak of the Se_n long chains in the A_{Se} mode.

Based on our experimental results of the local- and intermediate-range atomic ordering in the $\text{Ge}_x\text{Se}_{1-x}$ glass, which we have presented above, it is tempting to present the following speculation on the mechanism of the stiffness transition. In the stressed-rigid region $0.33 \geq x \geq 0.26$, some of the corner- and edge-sharing connections between the $\text{Ge}(\text{Se}_{1/2})_4$ tetrahedra are replaced by Se_2 dimers. In the resulting Ge-Se-Se-Ge units, the Ge-Se-Se bond angle is not larger than $\sim 90^\circ$. Such a small bond angle in Ge-Se-Se should possess a relatively high bonding stress and may be responsible for the higher-frequency contribution to the A_{Se} stretching mode.

With the decrease of x into the unstressed-rigid (*intermediate phase*) regime $0.26 \geq x \geq 0.20$, the stressful Se_2 dimer connections are replaced by longer Se_n ($n \geq 3$) chains, and the system rapidly reduces the fraction of the direct connections. With the further decrease of x into the floppy region $x \leq 0.20$, the tetrahedra are connected mainly by long Se_n chains and a small portion of the Se_1 monomers. The former connections completely release the stress in the intermediate-range structure to be the underconstraint floppy glass.

At a glance, this scenario of the phase-separation tendency between the tetrahedra and Se chains is similar to that described by Inam *et al.*²² and Chen *et al.*²³ Based on the *ab initio* MD results, they concluded that the concentrations of the short Se_n chains ($2 \leq n \leq 5$) connecting the $\text{Ge}(\text{Se}_{1/2})_4$ tetrahedra comprises maximum values between $0.20 \leq x \leq 0.23$ in the intermediate phase, as shown in Fig. 3(a) of Ref. 22. This reflects the *delayed* growth of the direct connections of corner- and edge-sharing tetrahedra with *increasing* x , as indicated in Fig. 3(b) of Ref. 22.

The present AXS results show another behavior for the x dependence of the Se_n concentrations. Although Se_3 , Se_4 , and Se_5 show weak maxima in the stiffness transition region, only the Se_2 dimer connections comprise a plateau in their x dependence, indicating that the system has a tendency to avoid Se_2 dimer connections between the tetrahedra. Also, the fraction of the direct connections, i.e., the Se_1 fraction in Fig. 11 shows a hump in the intermediate phase concentration range. From the present AXS results, it is thus concluded that with *increasing* x in the stiffness transition region, the connection growth of the direct connections between the tetrahedra is surely *delayed*. However, the delay is not caused by the fact that the system favors all of the short Se_n chain connections between the tetrahedra as concluded by Inam *et al.*²² but by avoiding the formation of the Se_2 dimer connections between the $\text{Ge}(\text{Se}_{1/2})_4$ tetrahedra.

Lucas *et al.*⁵⁴ carried out detailed nuclear magnetic resonance (NMR) and Raman-scattering studies on $\text{Ge}_x\text{Se}_{1-x}$ glasses ($0 \leq x \leq 1/3$) along a wide temperature range up to 520 K. They could not identify any Ge-Se-Se fragments in these glasses, and proposed a bimodal percolation model

based on intertwined domains of GeSe₂ and Se chains. The preference of Se-Se-Se connections over the Ge-Se-Se configurations in the stiffness transition region is consistent with our AXS+RMC results. However, the complete absence of Ge-Se-Se fragments in their model does not agree with the MD simulation results at $x = 0.20$ by Massobrio *et al.*⁴⁴ and Tafen and Drabold,⁵⁵ and the present experimental data. In a more recent NMR work by Gjersing *et al.*,⁵⁶ it is shown that Ge-Se-Se and Ge-Se-Ge fragments hardly can be discriminated by NMR. Therefore, detailed theoretical determinations of the NMR peak positions resulting from the Ge-Se-Se and Ge-Se-Ge sites are necessary to unravel these contradictory findings.

VI. CONCLUSION

In order to explore the relation between the short- and intermediate-range atomic structures and the stiffness transition in Ge_xSe_{1-x} glasses, the AXS experiments were performed close to the Ge and Se K absorption edges, and the resultant $\Delta_i S(Q)$ functions were analyzed using RMC modeling. The prepeak in $S(Q)$, indicating the existence of IRO, is not only composed of the Ge-Ge atomic correlations, but the Ge-Se and Se-Se also contribute to the prepeak. Although the obtained $S_{ij}(Q)$ and $g_{ij}(r)$ partials seem to gradually change with x , some indications related to the stiffness transition are found in the intermediate-range structure.

First, the preshoulder position in $S_{\text{SeSe}}(Q)$ largely shifts in the *intermediate phase* concentration range. Second, the Ge-Se-Se bond angles are distributed at $\sim 90^\circ$ in the transition region. No appreciable portions of the Ge-Se-Se-Ge sequences are found in the Ge_{0.20}Se_{0.80} glass. Instead, there is experimental evidence for a phase-separation tendency between directly connected Ge(Se_{1/2})₄ tetrahedra and Se _{n} ($n \geq 3$) chains in the *intermediate phase* region of the stiffness transition, which may be due to avoid large stress in the Se₂ dimer bonds, i.e., the small Ge-Se-Se bond angle. The present AXS experiment in combination with RMC modeling shows the excellent feasibility to obtain information on short- and intermediate-range atomic configurations in noncrystalline network glasses.

ACKNOWLEDGMENTS

We gratefully thank Professor P. Boolchand, Professor K. Murase, and Dr. D. Raoux for encouragement of this work and valuable discussion, and Professor C. Massobrio for providing the *ab initio* MD simulation data of glassy GeSe₂ and GeSe₄ and for discussion. This work was supported by the Deutsche Forschungsgemeinschaft (DFG), the Bundesministeriums für Bildung, Wissenschaft, Forschung und Technologie (Bmbf), and the Fonds der Chemischen Industrie. The AXS experiments were performed at the beamline BM02 in the ESRF (Proposals No. HS1562, No. HS1860, and No. HS2184).

*hosokawa@cc.it-hiroshima.ac.jp

†Former name, Yong Wang.

¹J. C. Phillips, *J. Non-Cryst. Solids* **34**, 153 (1979).

²M. F. Thorpe, *J. Non-Cryst. Solids* **57**, 355 (1983).

³W. A. Kamitakahara, R. L. Cappelletti, P. Boolchand, B. Halfpap, F. Gompf, D. A. Neumann, and H. Mutka, *Phys. Rev. B* **44**, 94 (1991).

⁴M. Taniguchi, T. Kouchi, I. Ono, S. Hosokawa, M. Nakatake, H. Namatame, and K. Murase, *J. Electron Spectrosc. Relat. Phenom.* **78**, 507 (1996).

⁵X. Feng, W. J. Bresser, and P. Boolchand, *Phys. Rev. Lett.* **78**, 4422 (1997).

⁶P. Boolchand, X. Feng, and W. J. Bresser, *J. Non-Cryst. Solids* **293–295**, 348 (2001).

⁷C. Peyrourou, S. Peytavin, and M. Ribes, *J. Solid State Chem.* **82**, 78 (1989).

⁸W. Zhou, M. Paesler, and D. E. Sayers, *Phys. Rev. B* **43**, 2315 (1991).

⁹E. Gulbrandsen, H. B. Johnsen, M. Endregaard, T. Grande, and S. Stølen, *J. Solid State Chem.* **145**, 253 (1999).

¹⁰J. C. Malenfant and J. Dixmier, *J. Non-Cryst. Solids* **35–36**, 1227 (1980).

¹¹T. Satow, O. Uemura, and Y. Sagara, *J. Jpn. Inst. Met.* **37**, 1348 (1973) (in Japanese).

¹²N. R. Rao, P. S. R. Krishna, S. Basu, B. A. Dasannacharya, K. S. Sangunni, and E. S. R. Gopal, *J. Non-Cryst. Solids* **240**, 221 (1998).

¹³Y. Wang, E. Ohata, S. Hosokawa, M. Sakurai, and E. Matsubara, *J. Non-Cryst. Solids* **337**, 54 (2004).

¹⁴D. Sharma, S. Samphath, N. P. Lalla, and A. M. Awasthi, *Physica B* **357**, 290 (2005).

¹⁵M. T. M. Shatnawi, C. L. Farrow, P. Chen, P. Boolchand, A. Sartbaeva, M. F. Thorpe, and S. J. L. Billinge, *Phys. Rev. B* **77**, 094134 (2008).

¹⁶Y. Waseda, *The Structure of Non-Crystalline Materials* (McGraw-Hill, New York, 1980).

¹⁷Y. Waseda, *Novel Application of Anomalous (Resonance) X-ray Scattering for Structural Characterization of Disordered Materials* (Springer, Heidelberg, 1984).

¹⁸Y. Waseda, *Anomalous X-Ray Scattering for Materials Characterization* (Springer, Heidelberg, 2002).

¹⁹P. Armand, A. Ibanez, Q. Ma, D. Raoux, and E. Philippot, *J. Non-Cryst. Solids* **167**, 37 (1993).

²⁰I. Petri, P. S. Salmon, and H. E. Fischer, *Phys. Rev. Lett.* **84**, 2413 (2000).

²¹S. Hosokawa, Y. Wang, J.-F. Béar, J. Greif, W.-C. Pilgrim, and K. Murase, *Z. Phys. Chem.* **216**, 1219 (2002).

²²F. Inam, D. N. Tafen, G. Chen, and D. A. Drabold, *Phys. Status Solidi B* **246**, 1849 (2009).

²³G. Chen, F. Inam, and D. A. Drabold, *Appl. Phys. Lett.* **97**, 131901 (2010).

²⁴S. Hosokawa, I. Oh, M. Sakurai, W.-C. Pilgrim, N. Boudet, and J.-F. Béar, *Phys. Status Solidi A* **206**, 1736 (2009).

²⁵R. L. McGreevy and L. Pusztai, *Molec. Simul.* **1**, 359 (1988).

²⁶R. L. McGreevy and M. A. Howe, *Ann. Rev. Mater. Sci.* **22**, 217 (1992).

²⁷O. Gereben, P. Jónvári, L. Temleitner, and L. Pusztai, *J. Optoelectron. Adv. Mater.* **9**, 3021 (2007).

²⁸Y. Waseda, S. Kang, K. Sugiyama, M. Kimura, and M. Saito, *J. Phys. Condens. Matter* **12**, A195 (2000).

- ²⁹S. Hosokawa and J.-F. Bélar, in *Ninth International Conference on Synchrotron Radiation Instrumentation*, AIP Conf. Proc. No. 879 (AIP, New York, 2007), p. 1743.
- ³⁰D. T. Cromer and D. A. Liberman, *J. Chem. Phys.* **53**, 1891 (1970).
- ³¹D. T. Cromer and D. A. Liberman, *Acta Crystallogr. Sect. A* **37**, 267 (1981).
- ³²S. Brennan and P. L. Cowan, *Rev. Sci. Instrum.* **63**, 850 (1992).
- ³³S. Sasaki, KEK Report 1989, National Laboratory for High Energy Physics, Tsukuba, 1989, p. 1 (unpublished).
- ³⁴S. Hosokawa, Y. Wang, M. Sakurai, J.-F. Bélar, W.-C. Pilgrim, and K. Murase, *Nucl. Instrum. Methods Phys. Res., Sect. B* **199**, 165 (2003).
- ³⁵M. Yoshizawa, S.-M. Zhou, R. Negishi, T. Fukamachi, and T. Kawamura, *Acta Crystallogr. Sect. A* **64**, 321 (2008).
- ³⁶S. Hosokawa, W.-C. Pilgrim, J.-F. Bélar, and S. Kohara, *Phys. Status Solidi A* (in press).
- ³⁷*International Tables for X-ray Crystallography*, 2nd ed., edited by C. H. MacGillavry and G. D. Rieck (Kynoch, Birmingham, 1968), Vol. III.
- ³⁸N. Metropolis, A. W. Rosenbluth, M. N. Rosenbluth, A. H. Teller, and E. Teller, *J. Phys. Chem.* **21**, 1087 (1953).
- ³⁹S. Kohara, K. Suzuya, Y. Kashihara, N. Matsumoto, N. Umesaki, and I. Sakai, *Nucl. Instrum. Methods Phys. Res., Sect. A* **467–468**, 1030 (2001).
- ⁴⁰S. Kohara and K. Suzuya, *Phys. Chem. Glasses C* **43**, 51 (2002).
- ⁴¹P. H. Fuoss, P. Eisenberger, W. K. Warburton, and A. Bienenstock, *Phys. Rev. Lett.* **46**, 1537 (1981).
- ⁴²S. Hosokawa, Y. Wang, W.-C. Pilgrim, J.-F. Bélar, S. Mamedov, and P. Boolchand, *J. Non-Cryst. Solids* **352**, 1517 (2006).
- ⁴³C. Massobrio and A. Pasquarello, *Phys. Rev B* **77**, 144207 (2008).
- ⁴⁴C. Massobrio, M. Celino, P. S. Salmon, R. A. Martin, M. Micoulaut, and A. Pasquarello, *Phys. Rev. B* **79**, 174201 (2009).
- ⁴⁵W. H. Zachariasen, *J. Am. Chem. Soc.* **54**, 3841 (1932).
- ⁴⁶P. S. Salmon, *J. Phys. Condens. Matter* **19**, 455208 (2007).
- ⁴⁷M. J. Haye, C. Massobrio, A. Pasquarello, A. De Vita, S. W. de Leeuw, and R. Car, *Phys. Rev. B* **58**, R14661 (1998).
- ⁴⁸A. L. Reninger and B. L. Averbach, *Phys. Rev. B* **8**, 1507 (1973).
- ⁴⁹J. Donohue, *The Structure of the Elements* (Wiley, New York, 1974).
- ⁵⁰G. Etherington, A. C. Wright, J. T. Wenzel, J. C. Dore, J. H. Clarke, and R. N. Sinclair, *J. Non-Cryst. Solids* **48**, 265 (1982).
- ⁵¹H. J. Trodahl, *J. Phys. C* **17**, 6027 (1984).
- ⁵²P. Tronc, *J. Phys. (Paris)* **51**, 675 (1990).
- ⁵³D. Selvanathan, W. J. Bresser, and P. Boolchand, *Phys. Rev. B* **61**, 15061 (2000).
- ⁵⁴P. Lucas, E. A. King, O. Gulbiten, J. L. Yarger, E. Soignard, and B. Bureau, *Phys. Rev. B* **80**, 214114 (2009).
- ⁵⁵D. N. Tafen and D. A. Drabold, *Phys. Rev. B* **71**, 054206 (2005).
- ⁵⁶E. L. Gjersing, S. Sen, and R. E. Youngman, *Phys. Rev. B* **82**, 014203 (2010).